SCIENCE CHINA
Earth Sciences

• RESEARCH PAPER •

March 2017 Vol.60 No.3: 463–477
doi: 10.1007/s11430-016-5082-6

A unified model of bidirectional reflectance distribution function for the vegetation canopy

XU XiRu[1,2], FAN WenJie[1,2*], LI JuCai[1,2], ZHAO Peng[1,2] & CHEN GaoXing[1,2]

[1] *Institute of Remote Sensing and Geographic Information System, Peking University, Beijing 100871, China;*
[2] *Beijing Key Laboratory of Spatial Information Integration & Its Applications, Beijing 100871, China*

Received August 1, 2016; accepted November 10, 2016; published online January 23, 2017

Abstract An accurate and operational bidirectional reflectance distribution function (BDRF) canopy model is the basis of quantitative vegetation remote sensing. The canopy reflectance should be approximated as the sum of the single scattering reflectance arising from the sun, ρ^1, and the multiple scattering reflectance arising from the canopy, ρ^m, as their directional characteristics are dramatically different. Based on the existing BRDF model, we obtain a new analytical expression of ρ^1 and ρ^m in this paper, which is suitable for different illumination conditions and different vegetation canopies. According to the geometrical optic model at the leaf scale, the anisotropy of ρ^1 can be ascribed to the geometry of the object, sun and the sensor, multiple scale clumping, and the fraction of direct solar radiation and diffuse sky radiation. Then, we parameterize the area ratios of four components: the sunlit foliage, sunlit ground, shadow foliage and shadow ground based on a Poisson distribution, and develop a new approximate analytical single scattering reflectance model. Assuming G=0.5, a recollision probability theory based scattering model is developed which considers the effects of diffuse sky radiation, scattering inside the canopy and rebounds between the canopy and soil. Validation using ground measurements of maize and black spruce forest proves the reliability of the model.

Keywords Vegetation BRDF, Unified model, Clumping Index, Proportion of direct solar radiation and diffuse sky radiation, Recollision probability

Citation: Xu X R, , Fan W J, Li J C, Zhao P, Chen G X. 2017. A unified model of bidirectional reflectance distribution function for the vegetation canopy. Science China Earth Sciences, 60: 463−477, doi: 10.1007/s11430-016-5082-6

1. Introduction

The solar radiance reflected by vegetation (0.3–2.5 μm) is bidirectionally reflected, and can be expressed by the bidirectional reflectance distribution function (BRDF),

$$\rho(\theta_i,\varphi_i,\theta_v,\varphi_v,\lambda)=\frac{L(\theta_v,\varphi_v,\lambda)}{\mu_i F(\theta_i,\varphi_i,\lambda)+E(\lambda)}. \quad (1)$$

In eq. (1), L is the radiance of an object received by the sensor, $\mu_i F$ and E are the irradiance of direct solar radiation and diffuse sky radiation, respectively, μ_i=cosθ_i, θ_i is the solar zenith angle, φ_i, θ_v, φ_v are the solar azimuth angle, viewing zenith angle and viewing azimuth angle, respectively, and λ is the wavelength. An accurate and operational canopy BRDF model is the priority for retrieving the leaf area index (LAI) from remote sensing data (Zhu et al., 2012). Numerous models have been developed, including the geometrical optic (GO) model and radiative transfer (RT) models, where computer simulations are the most popular BRDF models (Verhoef, 1984; Xu, 2005; Liang, 2005).

In the GO model the discrete vegetation is the object of study, the tree crown is assumed to have a regular geometry,

*Corresponding author (email: fanwj@pku.edu.cn)

and the crown and background surfaces are assumed to be Lambertian. Only directional solar radiation is considered, while the radiance received by the sensors is assumed to be composed of signals from four components: sunlit crown, sunlit ground, shaded crown and shaded ground. Their corresponding area ratios are denoted as K_c, K_g, K_t, K_z (Li and Strahler, 1985).

$$L = K_c L_c + K_g L_g + K_t L_t + K_z L_z, \quad (2)$$

L_c, L_g, L_t, L_z are the radiance of the sunlit crown, sunlit ground, shadow crown and shadow ground, respectively. If the crown is sparsely distributed in the receiver's pixels, K_c, K_g, K_t, K_z can be calculated according to geometric projection. Li and Strahler (1985) were the first to suggest that the combined geometry of the object, sun and the sensor was inferred as the main reason for anisotropic reflectance. This approach was able to successfully explain and simulate hot spots. Based on eq. (2), the four-scale GO model proposed that the tree distribution pattern and foliage distribution pattern within the trees were not random, and clumping on different scales had profound effects on the forest BRDF (Chen and Leblanc, 1997). Clumping can increase the gap fraction and change the area ratio of the above-mentioned four components and their contribution to multiple scatterings.

The GO model was challenged in several aspects: (1) it is difficult to calculate the area ratio of four components when the crowns are very dense. To date, it is still difficult to simplify the description of the clumping effect. (2) The crown surface is a solid sphere, and the normal direction of a surface element (ds) is changed, thus the irradiance of ds correspondingly changes. So the radiance reflected by a crown surface is non-Lambertian, even when the elements are solid spheres with Lambertian surfaces. (3) As the near-infrared band is indispensable to vegetation parameter retrieval, observed radiances arising from multiple scattering processes cannot be neglect (Chen and Leblanc, 1997). With these limitations in mind, how can we further the GO model to solve these challenges and hence improve the vegetation BRDF.

Based on the principle of energy conservation, the disciplinarian of energy transfer during the collision was established via RT modeling (Chandrasekhar, 1960). The precondition of the RT equation is that the radiation process is independent among the scattering particles. This can be established when the scale of the scattered particles is less than the wavelength (λ), and the space between scattering points is more than tenfold the wavelength, $D>10\lambda$ (Zhou et al., 1991). In another words, diffraction satisfies these conditions. RT models can successfully describe the interaction process between sunlight and the atmosphere as the main scatterers in the atmosphere are gas molecules and aerosols. Thus, no shadows and hot spots can be deduced according to RT modeling, thus contradicting the vegetation BRDF. Many studies tried to solve this problem, but all of these works focused on correlations between the four components in different directions, which were inherently based on the GO model (Jupp and Strahler, 1991; Kuusk, 1991). The integration of the GO model with RT modeling severely damaged the uniformity of their logical deductions. The existence of shadows and hotspots has proved that single-scattering reflectance obeys the geometrical optic model. According to random multiple scattering, ρ^m is isotropic, so that ρ^1 and ρ^m should be separated, hence: $\rho=\rho^1+\rho^m$.

Along with the rapid development of computer technology, the Monte Carlo method (MC) and the real-scenarios simulation algorithm were widely used to simulate the BRDF. Taking advantage of the inherent strengths of the computational environment, these methods were able to simulate real physical processes, and obtain an averaged result. These numerical simulation not only supported results obtained from field tests, but also provided a modeling reference database, but the model can't satisfy the request of very complicated conditions.

MC simulations track the continuous progress of photons, and simulate the ratio of absorption and scattering energy along a collision course (North, 1996; Xu, 2005); however, they do not consider the spatial distribution of the scattering radiation. Each photon course is repeated ten million times, just like the interaction between real photons and canopy, until a simulation result becomes stable. Thus, a precondition of the MC simulation is the independence of each tracking process. The ratio of scattering and absorption in the vegetation canopy depends on the optical properties of the vegetation elements (leaf single scattering albedo ω_l) and the recollision probability; however, it is unrelated to the vegetation illumination conditions (Knyazikhin et al., 1998, 2011). Thus, MC models are unable to simulate hotspots, and are also unable to simulate ρ^1, but they can be used to simulate ρ^m, as multiple scattering is approximately isotropic. Assuming G=0.5, the approximate solution of ρ^m can also be derived according to recollision probability.

The real-scenarios simulation model is composed of two parts: (1) the simulation of vegetation canopies, where many software programs can produce visually realistic vegetation canopies (Liang, 2005); and (2) the simulation of the process between electromagnetic waves and vegetation elements, such as ray-tracing methods and radiosity simulation methods, where the radiosity-graphics combined model (RGM) is a typical example of the latter method (Qin and Gerstl, 2000; Huang et al., 2013). When the location and spatial distribution of leaves are used as input, the area ratios of the four components can be calculated, and the distribution of irradiance in a scene can be simulated. In this approach, the BRDF of RGM can successfully simulate hotspots (Qin and Gerstl, 2000; Huang et al., 2013).

On the basis of analyzing and summarizing the existing models, we tried to explore the generality and individuality of various vegetation canopies. If G=0.5, and the reflectance

and transmittance of vegetation elements is approximately Lambertian, we found that different canopies can be unified by the clumping index and the gap fraction. According to GO model at the leaf scale, we parameterized a new approximate analytic single scattering reflectance model. A recollision probability theory based scattering model was also developed. The unified model was established to describe the bidirectional reflectance characteristics for different canopies and different illuminations.

2. The principles of the unified vegetation BRDF model

The canopy reflectance should be approximated as $\rho=\rho^1+\rho^m$, where ρ^1 represents the contribution of a single scattering reflectance, and ρ^m represents the multiple scattering reflectance (Qin and Jupp, 1993; Chen and Leblanc, 1997; Fan et al., 2014). Their directional characteristics in 2π space are dramatically different, where the former shows significant anisotropy, such as hotspots and the bowl edge effect, while the latter shows approximate isotropy. Their driving factors are also different, implying that their solving methods are also different. Then the contribution of sun light and the sky scattering to the canopy BRDF can be expressed accurately.

The radiance received by sensors can be expressed as $L=L^1+L^m$, where L^1 and L^m are the radiance received by the sensor from the vegetation-soil system through single scattering and the multiple scattering, respectively, $\rho^1=L^1/(\mu_i F_i+E)$, $\rho^m=L^m/(\mu_i F_i+E)$.

According to the GO model, L^1 can be expressed using eq. (2). However, in this paper the GO model was transferred from the crown scale to the leaf scale, where the four components are the sunlit foliage, the sunlit ground, the shadow foliage and the shadow ground, respectively. Their area ratios are denoted as K_c, K_g, K_t, K_z, respectively. If G=0.5, and the reflectance and transmittance of vegetation elements is approximately Lambertian, the reflected radiance of the four components is anisotropic, but we avoid the hypothesis that the vegetation element is Lambertian. The bidirectional gap fraction was derived instead from a Poisson distribution, and the clumping effect was also taken into account, so that we could calculate the clumping effect of dense vegetation. Then L_c, L_g, L_t, L_z can be approximately calculated analytically to describe the contribution from the sunlight and the sky scattering to the canopy BRDF.

L^m is the radiance caused by multiple scatterings, and it is nearly isotropy. $L^m=M^m/\pi$, M^m is exitance of the vegetation-soil system caused by multiple scatterings, where both the solar and sky scatterings are light sources. $M^m = u_i F_i \rho^m_{i\to\Omega} + E\rho^m_{\Omega\to\Omega}$, $\rho^m_{i\to\Omega}$ and $\rho^m_{\Omega\to\Omega}$ are the directional hemisphere and hemispherical reflectance of the vegetation canopy caused by multiple scatterings, respectively. $\rho^m = \left[(1-\beta)\rho^m_{i\to\Omega} + \beta\rho^m_{\Omega\to\Omega}\right]/\pi$, and we derived the analytical formulae when $\rho^m_{i\to\Omega}$ and $\rho^m_{\Omega\to\Omega}$ (Appendix 1, available at http://earth.scichina.com).

If the scattering phase function of the vegetation elements (such as leaves) can be expressed as the sum of the Lambertian reflectance and specular reflectance, and G=0.5, the reflectance and transmittance of elements can be approximated as Lambertian scatterings on the canopy scale. The escape probability of canopy photons is decided by the canopy gap fraction (Knyazikhin et al., 1998, 2011; Mõttus, 2007). Thus, the recollision probability depends on the vegetation structure, and the wavelength is irrelevant (Panferov et al., 2001; Stenberg, 2007; Huang et al., 2007). The ratio of ρ^1 and ρ^m, and hence $\rho^m_{i\to\Omega}$ and $\rho^m_{\Omega\to\Omega}$, can be calculated using recollision probability (Smolander and Stenberg, 2005; Fan et al., 2014).

3. The approximately analytical formula of ρ^1

3.1 The gap fraction

According to the Poisson distribution, the interception probability of a photon caused by foliage in 2-D space is $G_{i,v}LAI_a$ if the leaves are distributed randomly. The gap fraction of vegetation canopies in the ecosystem scale in the θ_i direction (Nilson, 1971) is,

$$P(\theta_{i,v}) = \mathrm{e}^{-\frac{G_{i,v}}{\mu_{i,v}}LAI_a}, \tag{3}$$

where G_i and G_v are the values of the G function in the solar direction and viewing direction, respectively, $\mu_i=\cos\theta_i$, $\mu_v=\cos\theta_v$, and LAI_a is the true average LAI of a pixel. In fact, vegetation elements that can intercept photons include foliage, branches, flower, spikes and so on. So, the LAI_a here is not the traditional leaf area index. Due to the complexities of non-leaf components, which do not possess characteristics in the 2-D plane, the plant area index (*PAI*), which should include the half leaf and non-leaf area per unit ground area, is introduced in this paper instead of the *LAI*.

For canopies distributed heterogeneously, the clumping index ξ can be used to modify eq. (3),

$$P(\theta) = \mathrm{e}^{-\xi(\theta)\frac{G}{\mu}\mathrm{PAI}}, \tag{4}$$

where $\xi(\theta)\dfrac{G(\theta)}{\mu}PAI$ is a dimensionless interception factor. The accuracies of $\xi(\theta)$ and *PAI* are crucial to eq. (4).

3.2 The relationship between ξ and θ

The pixel average *LAI* should not be affected by clumping. Instead, clumping will change the spatial distribution patterns of the considered canopies. It has been proven that the

pixel average gap faction will increase when clumping is considered. Thus, the clumping index $\xi \leq 1$. If canopies are distributed randomly in a pixel, and the total leaf area and pixel area are *LA* and *A*, respectively, then, $LAI_a=LA/A$. The gap fraction in the 0° viewing direction is $P(0)=e^{-GLAI_a}$.

If foliage are clustered and distributed randomly in the sub-pixel, whose area is a_1, then,

$$LAI_{a_1}=\frac{LA}{a_1}=\frac{A}{a_1}LAI_a. \tag{5}$$

The bare area of the pixel is a_2 ($a_2=A-a_1$). Thus, the average gap fraction of the pixel (*A*) can be expressed as,

$$\overline{P}(0)=P\left(LAI_{a,1}\right)+\frac{a_2}{A}\left[1-P\left(LAI_{a,1}\right)\right], \tag{6}$$

when $a_2=0$, $\overline{P}=P\left(LAI_{a,1}\right)=P\left(LAI_a\right)$, when a_2 is closed to *A*, $\overline{P}$ is closed to 1 (As shown in Figure 1). When a_2 increases from 0 to *A*, canopies will become more and more aggregated, and $\overline{P}$ will increase from $P(LAI_a)$ to 1 if $\partial\overline{P}/\partial a_2>0$. This shows that canopy aggregation can increase the pixel average gap fraction (details in Appendix 2).

So, how can we determine the two unknown parameters $\xi(\theta)$ and *PAI* in eq. (4)? For row crops, if the principal plane is perpendicular to the rows (as shown in Figure 2) and we set the unit distance in the *y* direction, then, $\mu_l=LA/(a_1\cdot H\cdot 1)$. The canopy gap fraction in the 0°-zenith-angle is,

$$P(0)=\frac{a_2}{A}\left(1-e^{-GLAI_1}\right)+e^{-GLAI_1}, \tag{7}$$

$$\xi(0)=-\frac{1}{GLAI_a}\ln P(0), \tag{8}$$

when $\theta=\theta_c$, $\theta_c=\tan^{-1}\left(\frac{A}{H}\right)$, then, θ_c is the crucial angle, and $\xi(\theta_c)=1$ (Appendix 3).

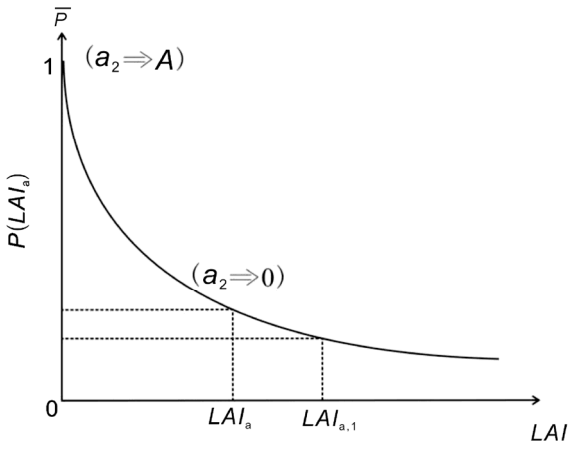

Figure 1 The relationship between pixel average gap fraction and canopy clumping.

When $\phi<(\pi/2)$, a_1, a_2 and *A* increase. When the value of θ_c increases to $\pi/2$, the relationship between $\xi(\theta)$ and θ is as shown in Figure 3 (Yan et al., 2012).

As discrete vegetation is distributed freely and randomly, it is hard to simulate the relationship between $\xi(\theta)$ and θ. Chen and Leblanc (1997) measured the gap fraction of black spruce canopies. The measured results showed that the measured gap fraction was closed to its simulated value derived from the Poisson formula when $\theta>15°$. When $\theta>7.5°$, $P(7.5°)$ can be calculated using a Newman distribution. The crucial angle was closed to 15° according to average tree height and distance among tree crowns. The measured results also showed that $\xi<1$ when $\theta<\theta_c$, and $\xi\cong 1$ when $\theta\geq\theta_c$, because gaps among tree crowns had disappeared. So, it could be approximated using a Poisson distribution. Accordingly, the relationship between $\xi(\theta)$ and θ shown in Figure 3 has general meaning.

Based on the relationship between $\xi(\theta)$ and θ, θ_c can be calculated when the vegetation canopy average height (*H*) and average distance among the tree crowns are obtained. If the G-value of non-leaf components are given (Müller-

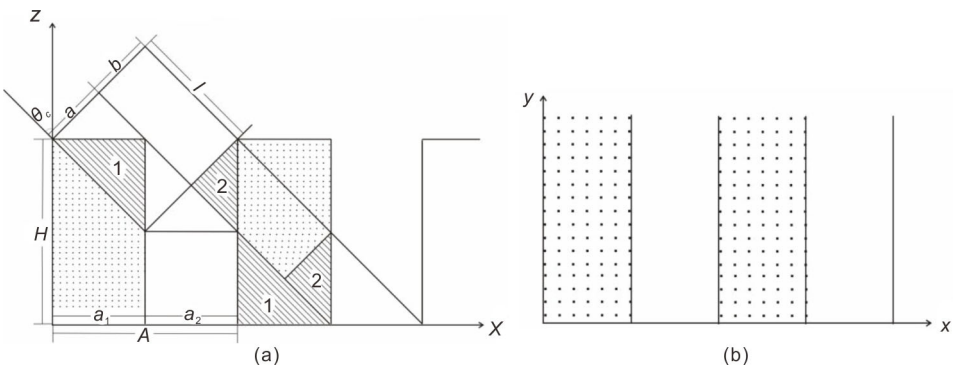

Figure 2 Vertical and horizontal sections of row crops.

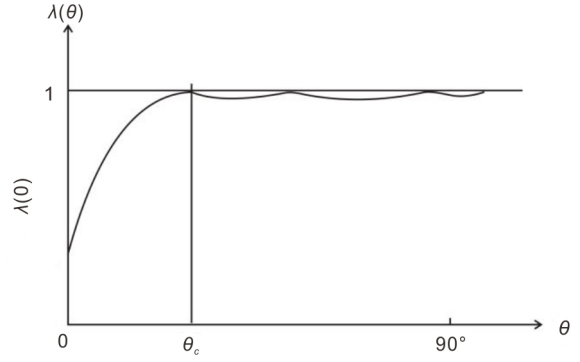

Figure 3 The relationship between $\xi(\theta)$ and θ (Yan et al., 2012).

Linow et al., 2015), the *PAI* can be retrieved using measured porosities when $\theta > \theta_c$ for $\xi(\theta) \cong 1$. Then $\xi(\theta)$ can be derived. According to this method, the pixel *PAI* of black spruce was 1.87 (G=0.5). The measured *LAI* of a single tree was 4.5 (Chen and Leblanc, 1997), and the pixel average true leaf area index (LAI_a) was 1.1451. The difference between *PAI* and LAI_a was caused by non-leaf components. So, it was different between the *LAI* retrieved by remote sensing methods and the traditional *LAI* (Chen and Leblanc, 1997). Because the contributions to BRDF coming from foliage reflectance and non-leaf components reflectance were disparate and the relationships between them and the four components (K_g, K_c, K_z, K_t) were complicated, components related to sunlit trunks and shaded trunks were added. In short, *PAI*s retrieved by remote sensing methods were different to the traditionally defined *LAI*s, and instead were close to the *PAI* values retrieved from the multi-angle measured gap fraction.

3.3 Four components calculation

3.3.1 Four components calculation formulae

If we set the land surface as the base level, the area ratios of the four components are the dimensionless interception probability of scattering. This is decided by the correlation between the gap fraction of the solar direction and the gap fraction of viewing direction (Figure 4).

Then, K_g can be expressed as,

$$K_g = \mathrm{e}^{-(l_i + l_v - l_c)} = \mathrm{e}^{-l_i} \cdot \mathrm{e}^{-l_v} \cdot \mathrm{e}^{l_c}, \tag{9}$$

where e^{-l_i}, e^{-l_v} are the gap fraction in the solar direction and viewing direction, respectively, and e^{l_c} describes the correlation of the two directions. Figure 5 shows how to calculate l_c.

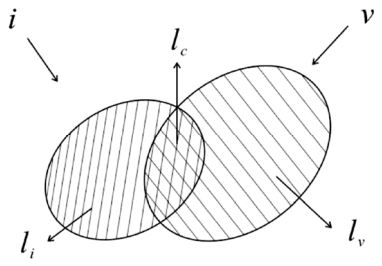

Figure 4 The effect of the correlation between the solar and viewing directions on the four components. Here i, v are the solar direction and viewing direction, respectively. The two ovals are the area ratios of the vegetation components projected to the land surface from the solar direction and the viewing direction, respectively. l_i, l_v are assumed to be dimensionless interception probabilities in the solar direction and viewing direction, respectively.

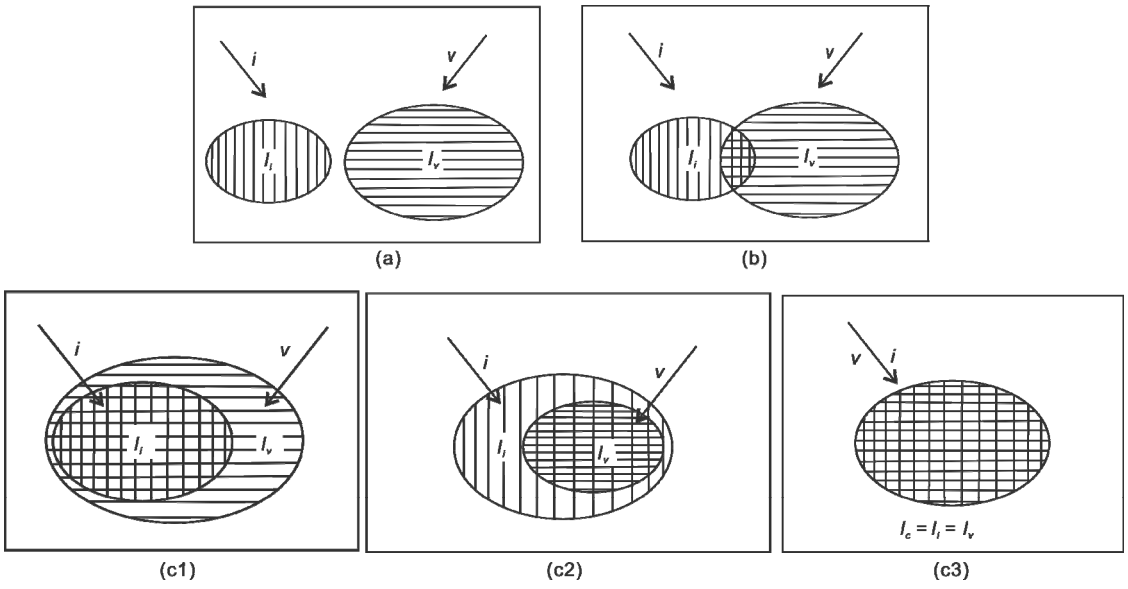

Figure 5 The l_c value. Where in a: l_c=0, in b: l_c is neither 0 nor maximum, and in c: l_c is maximum. When l_c=0, $K_g = e^{-l_i} \cdot e^{-l_v}$ This reveals that i and v are uncorrelated. In the cases of Figure 5, $l_i + l_v - l_c \geqslant 0$. So, $0 \leqslant \underset{(a)}{K_g} < \underset{(b)}{K_g} < \underset{(c)}{K_g} \leqslant 1$. When $PAI \to \infty$ or $\theta_{i,v} \to \pi/2$, $K_g \to 0$, when $PAI \to 0$, $K_g \to 1$.

According to the definitions of the four components,

$$\begin{aligned} &K_z+K_g=\mathrm{e}^{-l_v}\\ &K_c+K_t=1-\mathrm{e}^{-l_v},\\ &K_c+K_g+K_t+K_z=1. \end{aligned} \tag{10}$$

It is certain that all four components exist at the same time, which is the foundation of the GO model.

$$\begin{aligned} &K_g+K_t+K_z=\mathrm{e}^{-l_c}=1-K_c,\\ &K_c=1-\mathrm{e}^{-l_c}, \end{aligned} \tag{11}$$

$$K_z=\mathrm{e}^{-l_v}-K_g, \tag{12}$$

$$K_t=\left(1-\mathrm{e}^{-l_v}\right)-K_c=\mathrm{e}^{-l_c}-\mathrm{e}^{-l_v}, \tag{13}$$

According to eqs. (10)–(13), $0\le K_c, K_g, K_t, K_z\le 1$; K_c, K_g, K_t, K_z are the probabilities of occurrence of the four components, respectively; $K_c+K_g+K_t+K_z=1$, is necessary, but is not a sufficient condition to GO because the properties of light (i.e. the value of β and its variations) can affect the vegetation BRDF.

For the GO model, calculating l_c is a key problem, which is determined by the correlation between the solar direction and viewing direction. The l_c calculation is based on the Earth's surface. However, the reference planes of the dimensionless interception probabilities calculated in the solar and viewing directions are vertical to the two directions. So, it is required to transform the projections.

3.3.2 l_c calculation

The three determinants to l_c are the sizes of l_i and l_v, the shapes of l_i and l_v, and the distance between l_i and l_v. The sizes of l_i and l_v are decided by $\frac{\xi_{i,v}G_{i,v}}{\mu_{i,v}}PAI$. When $\theta_{i,v}=0$ and the shapes of l_i and l_v are assumed as round, their radii can be expressed as,

$$r_{i,v,0}=\sqrt{\frac{\xi(0)G(0)PAI}{\pi}}, \tag{14}$$

when $\theta_{i,v}\neq 0$, the shapes of l_i and l_v are still round in the planes which are perpendicular to the i or v directions. However, the projected shape on the surface should be elliptical. Its minor axis is still r_0, and the major axis should turn into $r_{i,v,l}$, as shown in Figure 6a

$$r_{i,v,l}=\frac{r_{i,v,0}}{\mu_{i,v}}, \tag{15}$$

a_i and a_v represent the central points of ellipse l_i and ellipse l_v the on x-axis, respectively, as shown in Figure 6b and then,

$$a_{i,v}=\frac{1}{2}H\mu_l\tan\theta_{i,v}, \tag{16}$$

here, $H=H_1+H_2$, where H_1 is the canopy thickness, and H_2 is the trunk height, and μ_l is the foliage volume density function (vegetation elements).

According to eq. (16), we should transform dimensional H (height) into a dimensionless one. Thus, it is crucial to determine the transformation relationships between them. The volume density function (μ_l) is introduced, and $\mu_l=LA/D$. Here, LA represents the total leaf area in the cylinder, D is the cylinder volume, and μ_l is still dimensional (i.e. $|L|^{-1}$). If $PAI=\mu_l\cdot H$, PAI will become dimensionless, and dimensional H can be transformed to a dimensionless variable using μ_l. Here $1/\mu_l$ is the correspondence value when the dimensionless variable is equal to 1. Then $H/(1/\mu_l)=H\mu_l=PAI$. The dimensionless factor should be $(H_1+H_2)\mu_l$ when vegetation canopies extend to the ground. When the solar and the viewing directions are both in the principal plane, the coordinates of the intersecting points (i.e., (x, y) in Figure 7) can be figured out through the two simultaneous elliptic equations mentioned before.

$$\frac{(x-a_i)^2\mu_i^2}{r_{i,0}^2}+\frac{y^2}{r_{i,0}^2}=1, \tag{17}$$

$$\frac{(x-a_v)^2\mu_v^2}{r_{v,0}^2}+\frac{y^2}{r_{v,0}^2}=1, \tag{18}$$

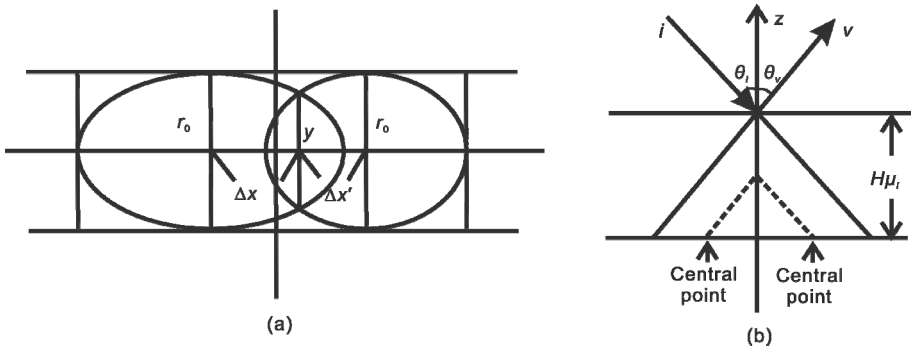

Figure 6 Sketches of overlay areas computations. (a) Vertical projection; (b) vertical cross-section.

where l_c, which consists of $l_{c,i}$ and $l_{c,v}$, is the overlay area of two projected ellipses in the i and v directions, as shown in Figure 7,

$$\left.\begin{aligned} l_{c,i} &= 2\cdot r_{i,0}\cdot r_{i,l}\cdot\left(\frac{1}{2}t_0-\frac{1}{4}\sin 2t\right)\\ l_{c,v} &= 2\cdot r_{v,0}\cdot r_{v,l}\cdot\left(\frac{1}{2}t_0-\frac{1}{4}\sin 2t\right)\\ \sin t &= \frac{|y|}{r_{i,v,\mathrm{o}}}, t=\sin^{-1}\frac{|y|}{r_{i,v,\mathrm{o}}} \end{aligned}\right\}, \tag{19}$$

where t_0 is the radian of t, and $t_0=\frac{t}{180^\circ}\cdot\pi$. When the intersection x is between a_i and a_v. In other situations, one value of t_0 can be still calculated using the method mentioned before, and the other, the updated t_0, should be $(\pi-t_0)$, which is determined by the actual locations of intersections of the two ellipses, especially the central points.

$l_{c,i}$ and $l_{c,v}$ in the horizontal plane have been expanded to $1/\cos\theta_i$ and $1/\cos\theta_v$, respectively, so,

$$l_c = l_{c,i}\cos\theta_i + l_{c,v}\cos\theta_v, \tag{20}$$

when the viewing direction is not in the principal plane, the computation method of l_c is showed in Appendix 4.

3.4 The ρ^1 approximate analytical expression considering skylight

$\rho_{v,\,i-v}$ and $\rho_{g,\,i-v}$ represent the directional-directional reflectance of foliage and soil, respectively. The diffuse reflectance, $\rho_{v,\,L}$ and $\rho_{g,\,L}$, are their average values. If diffuse scattering in the path of the incident light is ignored, the sunlit $L_c=\mu_i F_i \rho_{v,\,L}$ and $L_g=\mu_i F_i \rho_{g,\,L}$.

For shaded components, if $L_a^{\downarrow}$ represents the downward radiance of skylight, and its contribution to ground radiant flux in one direction should be $L_a^{\downarrow}\cdot\cos\theta_i\cdot \mathrm{e}^{-\frac{\lambda(\theta)GPAI}{\cos\theta_i}}\cdot\cos\theta_i \mathrm{d}\Omega$. Hence, the average contribution S_g in 2π space can be expressed as,

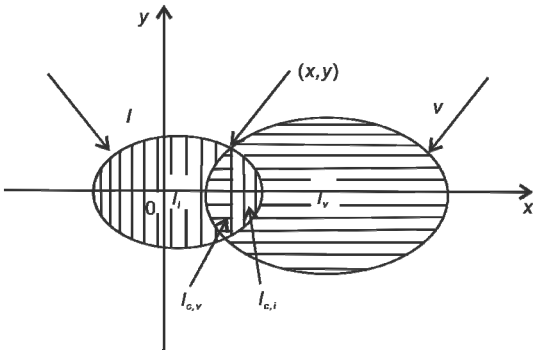

Figure 7 A sketch of $l_{c,i}$ and $l_{c,v}$ in the principal plane.

$$S_g=\frac{1}{2\pi}\int_{2\pi^+} L_a^{\downarrow}\cos\theta\cdot \mathrm{e}^{-\frac{\xi(\theta)GPAI}{\cos\theta}}\cos\theta \mathrm{d}\Omega. \tag{21}$$

Because $L_a^{\downarrow}\cos\theta$ and $\mathrm{e}^{-\frac{\xi(\theta)GPAI}{\cos\theta}}\cdot\cos\theta$ are uncorrelated,

$$\begin{aligned} S_g &= \int_{2\pi^+} L_a^{\downarrow}\cos\theta \mathrm{d}\Omega\cdot\frac{1}{2\pi}\int_{2\pi^+}\mathrm{e}^{-\frac{\xi(\theta)GPAI}{\cos\theta}}\cdot\cos\theta \mathrm{d}\Omega\\ &= E\int_0^{\frac{\pi}{2}}\cos\theta\sin\theta\cdot\mathrm{e}^{-\frac{\xi(\theta)GPAI}{\cos\theta}}\mathrm{d}\theta. \end{aligned} \tag{22}$$

Let $S'=\int_0^{\frac{\pi}{2}}\cos\theta\sin\theta\cdot\mathrm{e}^{-\frac{\xi(\theta)GPAI}{\cos\theta}}\mathrm{d}\theta$, then, $S_g=S'E$. $\rho_{g,\Omega\to v}$ represents the hemispherical-directional reflectance of the ground, then, $L_z=S'E\cdot\rho_{g,\Omega\to v}$. The average irradiance S_v to the vegetation canopy should be, $S_v=E-S'E=(1-S')E$, $L_t=(1-S')E\cdot\rho_{v,\Omega-v}$. Here, $\rho_{v,\Omega-v}$ is the average hemispherical-directional reflectance of the foliage. Let $\beta=\frac{E}{\mu_i F_i+E}$,

$$\begin{aligned} \rho^1 &= (1-\beta)K_g\rho_{g,i-v}+(1-\beta)K_c\rho_{v,i-v}\\ &\quad + S'\beta K_z\rho_{g,\Omega-v}+(1-S')K_t\rho_{v,\Omega-v}. \end{aligned} \tag{23}$$

This equation is based upon two approximations: (1) We ignore the effects of diffuse scattering in the sunlight path on sunlit components, and the direct sunlight has no contribution to the shaded components, and (2) we assume $\rho_{v,i-v}=\rho_{v,\Omega-v}=\rho_{v,L}$, $\rho_{g,i-v}=\rho_{g,\Omega-v}=\rho_{g,L}$.

Thus, the approximate analytical expression of ρ^1 should be,

$$\begin{aligned} \rho^1 &= (1-\beta)K_g\rho_{g,L}+(1-\beta)K_c\rho_{v,L}\\ &\quad + S'\beta K_z\rho_{g,L}+(1-S')\beta K_t\rho_{v,L}. \end{aligned} \tag{24}$$

4. Multiple scattering reflectance

4.1 Expression of the recollision probability

When the photons impinge upon a canopy at the zenith angle θ, some of them are intercepted by the vegetation element, where the probability of having two interactions with one photon within the canopy is called the one-time recollision probability (p^1). Because there is a negative exponential relationship between the gap fraction and $-\xi(\theta)G(\theta)LAI/\mu_\theta$, the photon interception probability also shows a negative exponential relationship with H, which means that more photons are intercepted by the upper layer of the canopy than by the lower layers, and intercepted photons have more chance to escape from the upper surface than the lower surface. This asymmetry effect directly re-

lates to the change of θ.

Assuming that N_0 photons are incident upon a canopy with solar zenith angle θ_i, and collide with the vegetation element at a depth of h, the amount of photons that escape from the upper surface, the bottom surface and remain in the canopy are $E'_{u,h}$, $E'_{d,h}$ and E'_h, respectively. The probabilities of photons from layer dh at a depth h that escape through canopy upwards, downwards and remain in the canopy are $q^1_{u,h}$, $q^1_{d,h}$ and e^1_h, respectively. The total photon escape and capture probabilities can be expressed as:

$$E^1_u=\int_0^H N_0 \mathrm{e}^{-\frac{\xi(\theta_i)G(\theta_i)u_l\cdot h}{\mu_i}}\cdot\frac{\xi(\theta_i)G(\theta_i)u_l}{\mu_i}\cdot\omega\cdot q^1_{u,h}\cdot \mathrm{d}h, \quad (25)$$

$$E^1_d=\int_0^H N_0 \mathrm{e}^{-\frac{\xi(\theta_i)G(\theta_i)u_l\cdot h}{\mu_i}}\cdot\frac{\xi(\theta_i)G(\theta_i)u_l}{\mu_i}\cdot\omega\cdot q^1_{d,h}\cdot \mathrm{d}h, \quad (26)$$

$$E^1=\int_0^H N_0 \mathrm{e}^{-\frac{\xi(\theta_i)G(\theta_i)u_l\cdot h}{\mu_i}}\cdot\frac{\xi(\theta_i)G(\theta_i)u_l}{\mu_i}\cdot\omega e^1_h\cdot \mathrm{d}h, \quad (27)$$

where Q^1_u, Q^1_d and p^1 represent the escaped probability of photons from the canopy upwards, downwards and recollide with the canopy, respectively, and their sum is 1. We have

$$\begin{aligned}
&E^1_u+E^1_d+E^1=N_0\omega(1-\mathrm{e}^{-\frac{\xi(\theta_i)G(\theta_i)u_lH}{\mu_i}}),\\
&Q^1_u=E^1_u/N_0\omega(1-\mathrm{e}^{-\frac{\xi(\theta_i)G(\theta_i)u_lH}{\mu_i}}),\\
&Q^1_d=E^1_d/N_0\omega(1-\mathrm{e}^{-\frac{\xi(\theta_i)G(\theta_i)u_lH}{\mu_i}}),\\
&p^1=E^1/N_0\omega(1-\mathrm{e}^{-\frac{\xi(\theta_i)G(\theta_i)u_lH}{\mu_i}}),\\
&p^1=1-(Q^1_u+Q^1_d),
\end{aligned} \quad (28)$$

where $q^1_{u,h}$ is the average gap fraction of the upper hemisphere, and $q^1_{d,h}$ is the average gap fraction of the bottom hemisphere, which can be expressed as:

$$q^1_{u,h}=\frac{1}{2\pi}\int_{2\pi^+}\mu_v \mathrm{e}^{-\frac{\xi(\theta_v)G(\theta_v)u_lh}{\mu_v}}\mathrm{d}\Omega_v, \quad (29)$$

$$q^1_{d,h}=\frac{1}{2\pi}\int_{2\pi^-}\mu_v \mathrm{e}^{-\frac{\xi(\theta_v)G(\theta_v)u_l(H-h)}{\mu_v}}\mathrm{d}\Omega_v, \quad (30)$$

$\xi(\theta_v)$ and $G(\theta_v)$ can be obtained from field measurements. Since $\mathrm{d}\Omega_i=\sin\theta_i\mathrm{d}\theta_i\mathrm{d}\phi_i$, $q^1_{u,h}$ and $q^1_{d,h}$ can be expressed as: $q^1_{u,h}=a\mathrm{e}^{-bh^c}$, $q^1_{d,h}=a\mathrm{e}^{-b(H-h)^c}$, where a, b and c are empirical parameters. When $\xi(\theta_v)=1$, $G(\theta_v)=0.5$ and $u_l=1$, the three parameters are 0.5, 1.1 and 0.8, respectively. Eq. (28) can be verified by MC simulations (Figure 8).

In Figure 8, the solid line represents the recollision probability derived from eq. (28), and the points represent the recollision probability derived from MC simulations. In the simulation, the leaf transmittance and reflectance were set to 0.44 and 0.4, respectively. The probabilities of photons to escape from the upper surface or bottom surface and remain in canopy after the first collision can be expressed as follows, respectively.

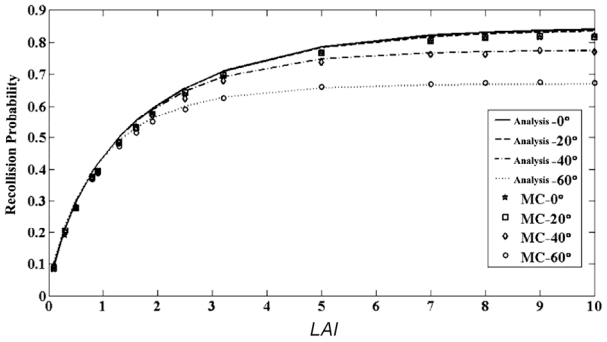

Figure 8 The relationship between p^1 and LAI for different incident angles.

$$\begin{aligned}
Q^m_u(LAI_a)&=\frac{0.5}{LAI_a\cdot 2\pi}\int_0^{LAI_a}\mathrm{d}h\int_{2\pi^+}\mathrm{e}^{-G(\theta_v)h/u_v}\mathrm{d}\Omega_v\\
&=\frac{0.5}{LAI_a}\int_0^{LAI_a}\mathrm{e}^{-bh^{0.8}}\mathrm{d}h,
\end{aligned} \quad (31)$$

$$Q^m_d(LAI_a)=\frac{0.5}{LAI_a}\int_0^{LAI_a}\mathrm{e}^{-b(H-h)^{0.8}}\mathrm{d}h, \quad (32)$$

$$p^m=1-(Q^m_u+Q^m_d)p^m. \quad (33)$$

The relationship between $Q^m_u(LAI_a)$ and $Q^m_d(LAI_a)$ and the relationship between p^m and LAI_a are shown in Figure 9.

4.2 Analytical expression of the multiple scattering reflectance

The interaction between radiation and the canopy can be divided into two separate processes (Figure 10): (1) photons are absorbed and scattered in the canopy when the ground

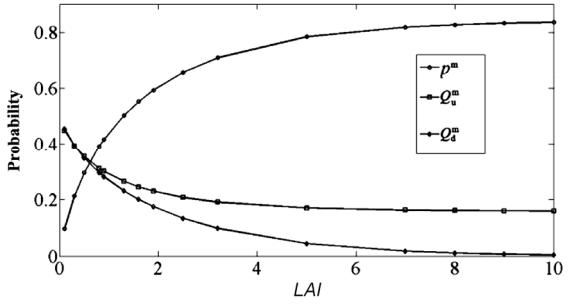

Figure 9 The relationship between $Q^m_u(LAI_a)$ and $Q^m_d(LAI_a)$, and the relationship between p^m and LAI_a.

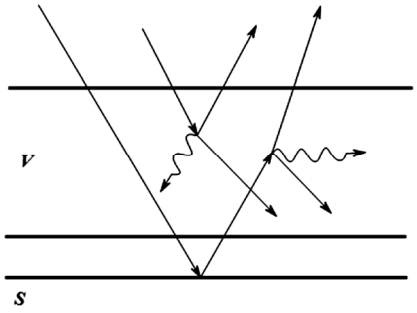

Figure 10 Absorption and scattering of photons in a vegetation soil system.

reflectance is zero, ρ_g=0; and (2) photons rebound between the canopy and the ground multiple times, and are then absorbed or scattered by the canopy when the ground reflectance is not zero ($\rho_g \neq 0$). Therefore, taking the effect of diffuse sky radiation and multiple photon scatterings into account, the multiple scattering reflectance can be approached as a sum of six parts.

4.2.1 Multiple scattering reflectance when ground reflectance equals zero

When ρ_g=0, the sum of the probabilities of the total scattering ($S_{\mathrm{bsD}}(\lambda)$) and the total absorption ($a(\lambda)$) of direct radiation can be expressed as:

$$S_{\mathrm{bsD}}(\lambda,\theta_i)+\alpha(\lambda,\theta_i)=i_0(\theta_i), \tag{34}$$

where the canopy interception probability is $i_0(\theta_i)=1-\mathrm{e}^{-\frac{\xi_i G_i LAI_a}{\mu_i}}$. Therefore, multiple scatterings of direct radiation in the canopy can be expressed as:

$$S^m_{\mathrm{bsD}}(\theta_i)=i_0\frac{\omega_l^2 p^1\left(1-p^m\right)}{1-\omega_l p^m}, \tag{35}$$

where ω_l is single leaf albedo. With the approximation $p^1=p^m=p$, then,

$$S_{bsD}{}^m(\theta_i)=i_0(\theta_i)\omega_l{}^2\frac{p(\theta_i)(1-p)}{1-\omega_l p}. \tag{36}$$

In fact, the effect of p^1 is bigger than p^m. As the value of p^m is related to θ_i, p can be expressed as a empirical function of θ_i. Assuming that G=0.5, the reflectance and transmittance of leaves in the canopy have Lambertian characteristics, and the multiple scattering is approximately isotropic. Hence, the probability that photons escape from the upper and bottom surfaces after the first collision can be both expressed as:

$$\frac{1}{2i_0}S^m_{bsD}=\frac{1}{2}\frac{\omega_l^2 p(1-p)}{1-\omega_l p}, \tag{37}$$

when ρ_g=0, the multiple scattering reflectance related to direct solar radiation then escapes upwards after being scattered more than once in the canopy is represented by ρ_1^m (Figure 11). The direct solar radiation is intercepted by the sunlit surface of leaves. The average irradiance of the leaves is $\mu_i F$. ρ_1^m can be expressed as:

$$\rho_1^m(\theta_i)=\left(1-\beta(\theta_i)\right)i_0(\theta)\frac{1}{2}\frac{\omega_l^2 p(1-p)}{1-\omega_l p}\frac{1}{\pi}, \tag{38}$$

when ρ_g=0, the multiple scattering reflectance due to diffuse sky radiation is represented by ρ_2^m. Diffuse sky radiation only interacts with shady leaf surfaces. The average irradiance by diffuse sky radiation is $E(1-S^{'})$. When i_0 replaced by $\tilde{i}_0$, where $\tilde{i}_0=\frac{1}{2\pi}\int_{2\pi} i_0 \mathrm{d}\Omega$, the formula to calculate ρ_2^m is derived as follows.

$$\rho_2^m=\beta\left(1-S^{'}\right)\tilde{i}_0\frac{1}{2}\frac{\omega_l^2 p(1-p)}{1-\omega_l p}\frac{1}{\pi}, \tag{39}$$

here the fraction of diffuse sky radiation to total radiation is expressed as $\beta=\frac{E}{\mu_i F+E}$, where $\mu_i F$ and E represent the average irradiance by direct solar radiation and diffuse sky radiation, respectively.

4.2.2 Multiple scattering reflectance when considering the ground

The direct solar radiation and diffuse sky radiation should be considered separately when the ground reflectance is not zero. For direct solar radiation, photons that interact with soil and then escape from upper surface can be divided into two parts (Figure 12): (1) for the photons that transmit through gaps to ground, and are then scattered upwards by canopy after rebounds between the canopy and ground, their reflectance is represented by ρ_3^m. Similar to ρ_3^m, the reflec-

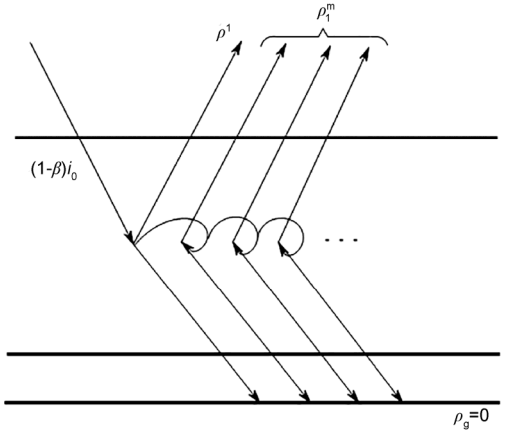

Figure 11 Schematic diagram of ρ_1^m.

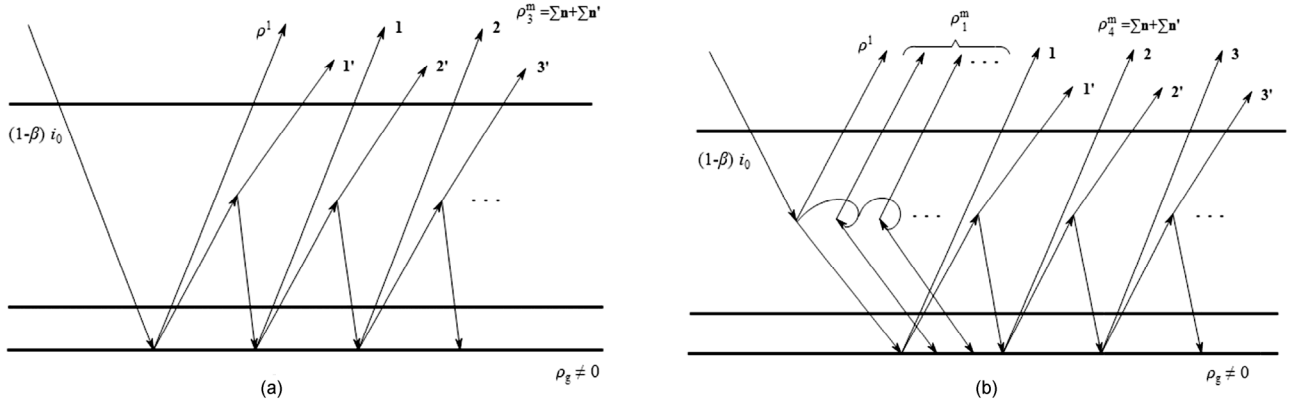

Figure 12 Schematic diagram of ρ_3^m and ρ_4^m.

tance caused by photons that transmit through the canopy are rebounded by the ground, then transmit through the canopy directly can be expressed as $(1-\beta)(1-i_0(\theta_i))\rho_g\left(1-\tilde{i}_0\right)$, which is a part of ρ^1. (2) Photons are intercepted by the canopy, then scattered upwards by the canopy after being scattered more than once between the canopy and the ground. Their reflectance is represented by ρ_4^m. Photons transmitted into the canopy can also escape after a single or multiple scattering in the canopy without reaching ground. They are related to ρ^1 or ρ_1^m respectively.

ρ_3^m is composed of two parts, and can be expressed as follows:

$$\begin{aligned}\rho_3^m &= \frac{1}{\pi}\left(\sum n+\sum n'\right)\\ &= (1-\beta)(1-i_0)\frac{\rho_g \tilde{i}_0 r_c^*}{1-\rho_g \tilde{i}_0 r_c^*}\left(1+\rho_g\left(1-\tilde{i}_0\right)\right)\frac{1}{\pi}.\end{aligned} \tag{40}$$

$$r_c^* = \frac{1}{2\tilde{i}_0}S_{bs}. \tag{41}$$

Similar to ρ_3^m, ρ_4^m can be calculated according to the following equation:

$$\begin{aligned}\rho_4^m &= \frac{1}{\pi}(\sum n+\sum n')\\ &= (1-\beta) i_0 r_c^* \frac{\rho_g}{1-\rho_g \tilde{i}_0 r_c^*}\left(1-\tilde{i}_0+\tilde{i}_0 r_c^*\right)\frac{1}{\pi}.\end{aligned} \tag{42}$$

The reflectance related to diffuse sky radiation that is transmitted through the canopy, rebounds between the canopy and the ground, and escapes upward from the canopy is ρ_5^m. The reflectance related to diffuse sky radiation that is transmitted to the ground, and rebounds between the canopy and the ground, and escapes upward is ρ_6^m. Each of these can be calculated according to the equations below, respectively.

$$\rho_5^m = \beta\cdot S'\left(1-\tilde{i}_0\right)\frac{\rho_g \tilde{i}_0 r_c^*}{1-\rho_g \tilde{i}_0 r_c^*}\left[1+\rho_g\left(1-\tilde{i}_0\right)\right]\frac{1}{\pi}, \tag{43}$$

$$\rho_6^m = \beta(1-S')\frac{\tilde{i}_0 r_c^* \rho_g}{1-\rho_g \tilde{i}_0 r_c^*}\left[1-\tilde{i}_0+\tilde{i}_0 r_c^*\right]\frac{1}{\pi}. \tag{44}$$

The multiple scattering reflectance is the sum of these six parts:

$$\rho^m = \rho_1^m+\rho_2^m+\rho_3^m+\rho_4^m+\rho_5^m+\rho_6^m. \tag{45}$$

4.2.3 *Analysis of the change pattern of* ρ^m

PAI is a key parameter that describes the canopy's characteristics and affects the multiple scattering reflectance. For an infinite horizontal canopy, the multiple scattering reflectance increases at first, along with an increase in *PAI*. Then, the multiple scattering reflectance increases at a declining rate. After reaching a maximum value, it keeps stable or declines slightly. The change of the multiple scattering reflectance and its six parts along with an increase in *PAI* is shown in Figure 13a.

Clumping can also change the gap fraction greatly, and it is an important influential factor for multiple scatterings. The clumping index determines the change pattern of the multiple scattering reflectance along with an increase of *PAI*. As Figure 13b shows, the bigger the clumping index is, the sooner the multiple scattering reflectance reaches its maximum value. The difference in the change patterns is mainly caused by ρ_1^m, ρ_2^m, ρ_3^m and ρ_4^m. The fraction of ρ_5^m and ρ_6^m to the total amount is very limited, which is about one tenth of ρ_3^m and ρ_4^m. Therefore, the effect of ρ_5^m and ρ_6^m can be neglected.

Single leaf albedo affects the multiple scattering reflectance remarkably. According to simulations, ρ^m increases greatly as ω_l increases from 0.2 to 0.8, and the maximum

value can increase by a factor of 20 (Figure 14a). The six parts of ρ^m affect the change of the total amount differently. ρ_1^m plays the most important role, and as Figure 14b shows, the summit value of ρ_1^m increases by a factor of 3, as ω_l changes from 0.2 to 0.8. The contributions of ρ_2^m, ρ_3^m and ρ_4^m are smaller than ρ_1^m by one order of magnitude. The contributions of ρ_5^m and ρ_6^m are smaller than ρ_2^m by one order of magnitude, and amount to less than 2% of the total amount, hence they can be neglected.

Ground reflectance affects the multiple scattering reflectance greatly under low *PAI* conditions, especially when *PAI* is in the range of 0 to 4. Along with a ground reflectance increase from 0 to 0.5, the multiple scattering reflectance increases dramatically when *PAI*=1 (Figure 15). ρ_3^m and ρ_4^m determine the change of ρ^m caused by different ground reflectance. While the effects of ρ_5^m and ρ_6^m are limited, the contribution of ρ_5^m and ρ_6^m to total amount is about one tenth of ρ_3^m and ρ_4^m, therefore they can be neglected. ρ_1^m and ρ_2^m are related to radiance that does not reach the ground, and they do not change along with the ground reflectance.

The multiple scattering reflectance of a homogeneous canopy increases slightly along with an increase in the solar zenith angle, as Figure 16 shows. The solar zenith angle describes direct solar radiation. Therefore, the effect of the solar zenith angle on the multiple scattering reflectance will be more slight when β increases.

β describes the fraction of direct solar radiation. When β is small, ρ_5^m and ρ_6^m can be neglected. Along with the increase of β, the multiple scattering reflectance related to diffuse radiation will be increasingly closer to that of direct radiation. When β=0.5, ρ_2^m, ρ_5^m and ρ_6^m are approximately the same as ρ_1^m, ρ_3^m and ρ_4^m, respectively. Simulation results indicate that direct radiation and diffuse radiation play quite similar roles to producing multiple scattering radiation. Actually, the portion of ρ_5^m and ρ_6^m in ρ^m are more than 20% (Figure 17) when β reaches 0.4. Therefore, they cannot be neglected in this situation.

4.2.4 *Approximation of* ρ^m

According to the analysis, the six parts of the multiple scattering reflectance can be merged to three parts:

$$\rho^m=\rho_1+\rho_2+\rho_3, \tag{46}$$

$$\rho_1=\left(\frac{i_0}{2}+\beta\left(\frac{\tilde{i}_0}{2}-S'\frac{\tilde{i}_0}{2}-\frac{i_0}{2}\right)\right)\frac{\omega_l^2 p(1-p)}{1-\omega_l p}\cdot\frac{1}{2\pi}, \tag{47}$$

ρ_1 is the sum of ρ_1^m and ρ_2^m. When β is smaller than 0.4, ρ_5^m and ρ_6^m can be neglected. Then ρ_2 and ρ_3 can be ap-

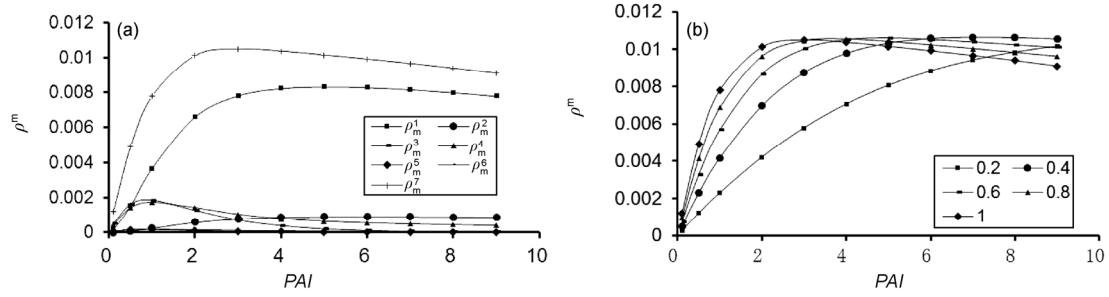

Figure 13 (a) The change of the multiple scattering reflectance and its six parts along with an increase of *PAI*, (b) The effect of the clumping index on the multiple scattering reflectance. ω_l=0.6, ρ_g=0.2, θ_i=30°, β=0.1.

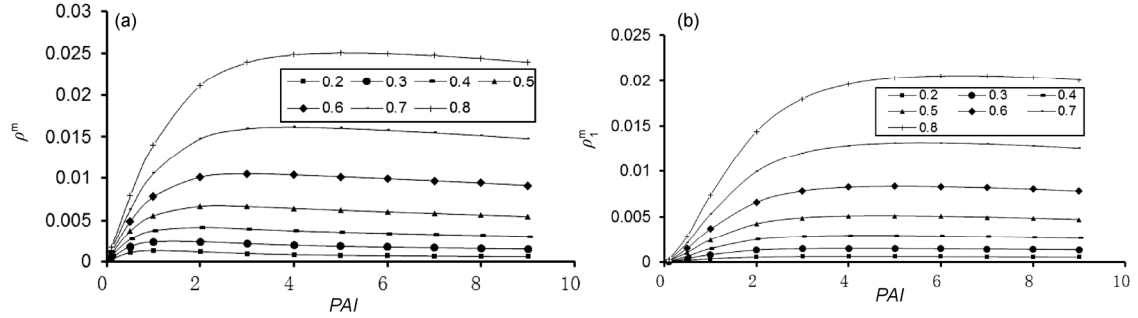

Figure 14 (a) The effect of single leaf albedo on the multiple scattering reflectance, (b) the effect of single leaf albedo on ρ_1^m. β=0.1, ρ_g=0.2, θ_i=30º.

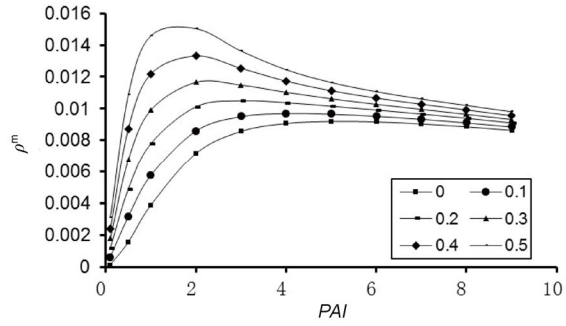

Figure 15 The effect of ground reflectance on the multiple scattering reflectance. ω_l=0.6, β=0.1, θ_i=30º.

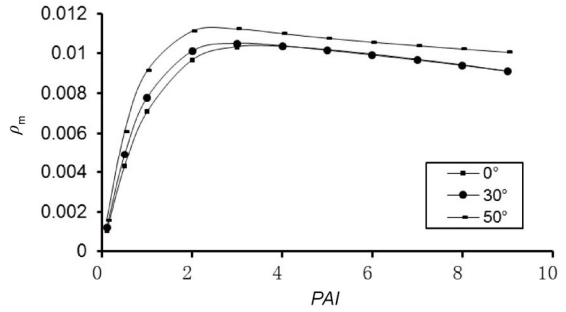

Figure 16 The multiple scattering reflectance at different solar zenith angles. ω_l=0.6, β=0.1, ρ_g=0.2.

proximated as,

$$\rho_2 = (1-\beta)(1-i_0)\frac{\rho_g \tilde{i}_0 r_c^*}{1-\rho_g \tilde{i}_0 r_c^*}\left(1+\rho_g\left(1-\tilde{i}_0\right)\right)\frac{1}{2\pi}, \quad (48)$$

$$\rho_3 = (1-\beta)\frac{i_0}{2}\frac{\omega_l(1-p)}{1-\omega_l p} \cdot \frac{\rho_g}{1-\rho_g \tilde{i}_0 r_c^*}\left(1-\tilde{i}_0\left(1-0.5\frac{\omega_l(1-p)}{1-\omega_l p}\right)\right)\frac{1}{2\pi}. \quad (49)$$

When β becomes 0.4 or greater, ρ_2 is the sum of ρ_3^m and ρ_5^m, ρ_3 is the sum of ρ_4^m and ρ_6^m. They can be expressed as:

$$\rho_2 = \left(1-i_0+\beta\left(S^{'}-S^{'}\tilde{i}_0-1+i_0\right)\right) \cdot \frac{\rho_g \tilde{i}_0 r_c^*}{1-\rho_g \tilde{i}_0 r_c^*}\left(1+\rho_g\left(1-\tilde{i}_0\right)\right)\frac{1}{2\pi}, \quad (50)$$

$$\rho_3 = \frac{i_0}{2}\left(1-\beta S^{'}\right)\frac{\omega_l(1-p)}{1-\omega_l p} \cdot \frac{\rho_g}{1-\rho_g \tilde{i}_0 r_c^*}\left(1-\tilde{i}_0\left(1-0.5\frac{\omega_l(1-p)}{1-\omega_l p}\right)\right)\frac{1}{2\pi}. \quad (51)$$

5. Results and discussion

5.1 The unified model experimental validation

We used the field measured BRDF data of maize canopies in Zhangye, Gansu Province obtained on July 1st, 2008, which belongs to one of the scientific achievements in the Heihe Watershed Allied Telemetry Experimental Research (WATER), to validate our model. The maize was in the time of closing. The synchronously measured canopy structure and other environmental parameters are listed in Table 1, and the simulated and measured values are showed in Figure 18.

We used the data collected by Chen and Leblanc (1997) of discrete forests to validate the unified BRDF model. The main vegetation type was black spruce. The field measured canopy structure and other environmental parameters are also listed in Table 1. Here, *LAI* was derived from a single tree *LAI* and the number of trees, which was the pixel average leaf area index. *PAI* is the plant area index, which

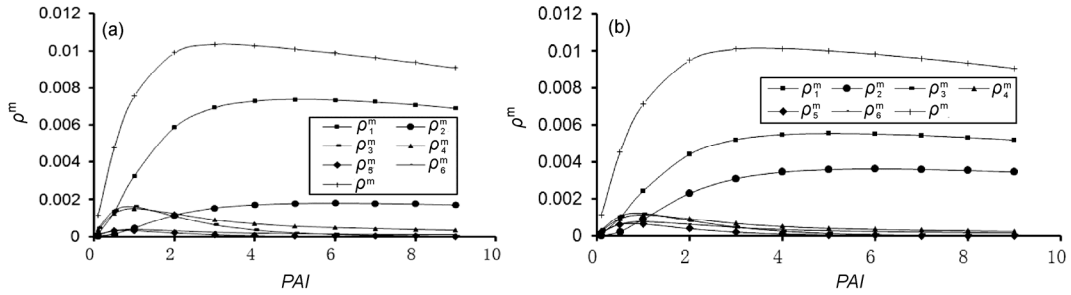

Figure 17 The multiple scattering reflectance and its six parts for different β. (a) β=0.2, (b) β=0.4, ω_l=0.6, β=0.1, θ_i=30º.

Table 1 The input parameters to the unified BRDF model

Vegetation	a_1(m)	a_2(m)	H(m)	LAI	$G(\theta)$	θ_i	φ_i	φ_v	β	$\rho_{v,red}$	$\rho_{g,red}$	$\rho_{v,nir}$	$\rho_{g,nir}$
Maize	0.48	0.14	1.52	4.52	0.5	27°	13°	10°	0.3	0.078	0.14	0.40	0.22
	H_1(m)	H_2(m)	PAI_a	LAI_a	$G(\theta)$	–	–	–	β	$\rho_{v,red}$	$\rho_{g,red}$	$\rho_{v,nir}$	$\rho_{g,nir}$
Black spruce	6.5	0.5	1.87	1.145	0.5	–	–	–	0.15	0.13	0.06	0.53	0.2

considers non-leaf elements such as trunks, and was obtained from the *LAI*. The diameter at breast height and other relevant parameters, including the ratio of sky scatterings, was acquired through measurements. The simulated and measured BRDF results are shown in Figure 19.

From Figures 18 and 19, it can be seen that the unified BRDF model can be effectively applied to crops and forest canopies. For row crops, the differences between the simulated values and measured values are obvious for some zenith angles (Figure 18). Because observed objects are corn planted by humans with a low degree of homogeneity, the field of view for ground multi-angle observation platform is so narrow that its stability cannot meet the experiments' requirements. The main input parameters, such as a_1(m), a_2(m), *LAI* and *G*, can only be acquired through traditional field measurements rather than through remote-sensing methods nowadays. If these parameters do not match with the scales of the remote sensing data, it will introduce errors to the results for heterogeneous vegetation (Zhang et al., 2010).

5.2 Effects of direct sunlight and sky scattering on the vegetation BRDF

The ratio of direct sun light and scattered light was decided by atmospheric transmittance. The less the atmospheric transmittance is, the less the amount of $\mu_i F_i$ that reaches the ground. When the amount of scattering increases, β also increases. The atmospheric scattering path increases along with an increase of θ_i; however, the total scattering $\mu_i F_i$ decreases. The field measured BRDF of black spruce indicates that the hot spot value when θ_i=−50° was smaller than measurements when θ_i=−40°, and bowl edge effects increases (Chen and Leblanc, 1997). β is a function of θ_i, implying it was the cause of the anisotropy radiances of the four components, even if we assumed the components were Lambertian.

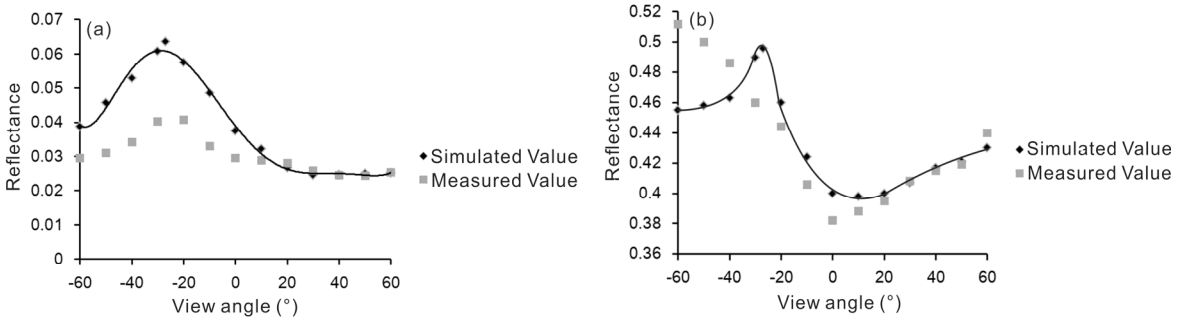

Figure 18 The comparisons between simulated and measured results for the corn canopies. (a) Red band; (b) near-infrared band.

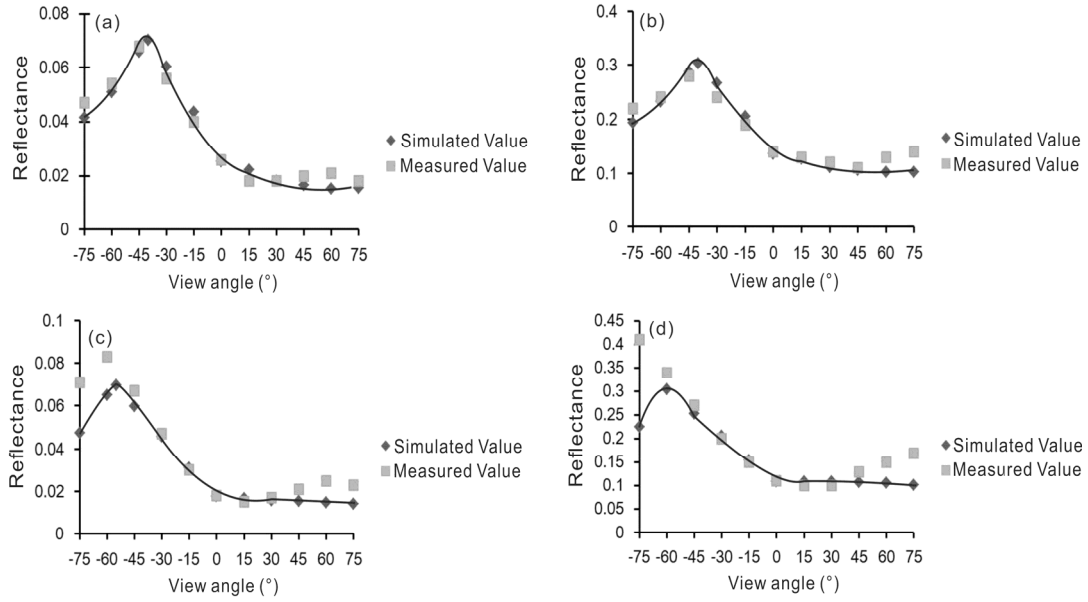

Figure 19 The comparisons between simulated and measured results of discrete forest canopies. (a) Red band (θ_i=−40°); (b) near-infrared band (θ_i=−40°); (c) Red band (θ_i=−55°); (d) near-infrareD band (θ_i=−60°).

Changes in wavelength could lead to the variations of $\mu_i F_i$ and E, when λ>0.5 μm. The sun could be regarded as a black body with a temperature of 6000 K, and its radiation is proportional to λ^{-5}. However, atmospheric molecular scattering is proportional to λ^{-4}, and aerosol scattering is proportional to λ^{-3}~λ^{-1}. So, β_{nir}>β_{red}, and the hot spot intensity in the near-infrared band was weaker than it was in the red optical band; however, bowl edge effects do the opposite. The measured black spruce BRDF data proved the relationship between $\mu_i F_i$ and E on the vegetation canopy BRDF. Next, numerical simulations were carried out (Figure 20).

We assumed $\xi_i \cong 1$, G=0.5 and PAI=1.87, and let b=$G_i LAI_e$, x=μ_i, K=0.5867. The solar zenith angle was −40°, and the viewing zenith angle ranged from −75° to 75° with intervals of 15°. The value β in the red optical band ranged from 0.1 to 0.5, with intervals of 0.05. The value of β in the near-infrared band ranged from 0.1 to 0.5, with intervals of 0.05. The reflectance for the different bands are listed in Table 2. The relationships between β and BRDF in the principal plane are shown in Figure 20, which proves that the effects of β on the vegetation BRDF cannot be ignored.

5.3 Effects of the clumping index on ρ^1

For similar vegetation types, different clumping indices will lead to different gap fractions. Thus, ρ^1 will be disparate. The relevant parameters measured by Chen and Leblanc (1997) were used to determine the relationships between ρ^1_{red} and ξ when θ_i=−40° and θ_v=−40°. The discrete vegetation PAI=1.87, LAI=1.145, the total height and canopy height of trees were H=7 m and H=6.5 m, respectively. The clumping index ranged from 0.1 to 1, with intervals of 0.1. The ρ^1 of hot spots was figured out under different clumping indices (as shown in Figure 21). It is essential for vegetation BRDF to obtain an accurate clumping index.

6. Conclusion

The unified model of BRDF for vegetation canopy has several characteristics: (1) it is based on vegetation element, and provides an approximate analytical expression of the vegetation BRDF and makes the inversion of vegetation indexed more convenient. (2) The model considers the BRDF as the sum of the single scattering reflectance and the multiple scattering reflectance, and calculates these two parts separately. It is helpful to understand vegetation BRDF intensively. (3) Unity is the most remarkable feature of the model, which means it can be applied to many kinds of vegetation in the spectral range from 0.3 to 2.5 μm. The model can also be applied to different atmospheric conditions. It provides a chance for the application of quantitative vegetation remote sensing model in the global change simulation.

The unified BRDF model has been preliminarily established. A large amount of measured data are now needed to verify this model. This will be our work in the future. The purpose of this model is to calculate the leaf area index. The unified model is an analytical model, suitable for different kinds of vegetation, and the input parameters are limited. Our next step will be to use an efficient inversion method for different vegetation indexes to take advantage of the model.

However, some canopy structural parameters, such as plant height and the value of G function, are difficult to obtain from passive visible light remote sensing. Instead, these indexes are usually obtained from field measurements or empirical knowledge. This then limits the application of

Table 2 Reflectance of components

	Red band	Near-infrared band
Foliage reflectance (ρ_v)	0.13	0.53
Ground reflectance (ρ_g)	0.06	0.20

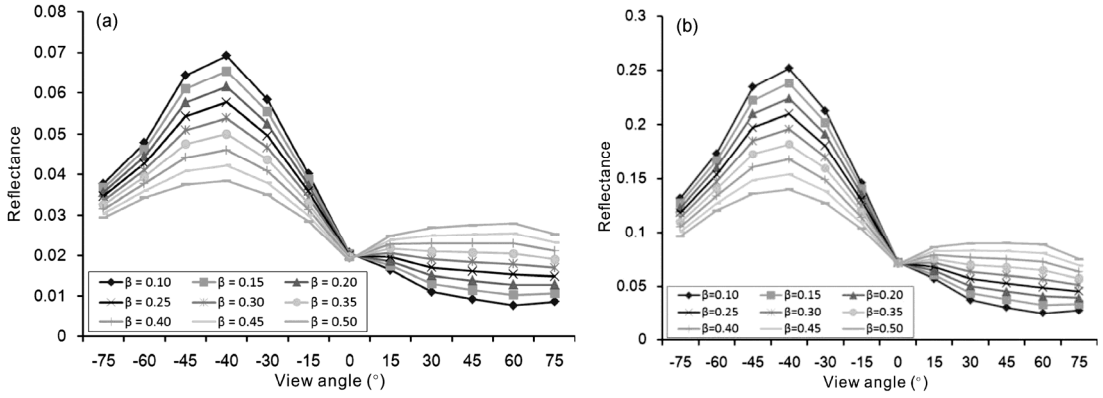

Figure 20 The relationships between β and BRDF in principal plane. (a) Red band; (b) near-infrared band. (a) Red band; (b) near-infrared band.

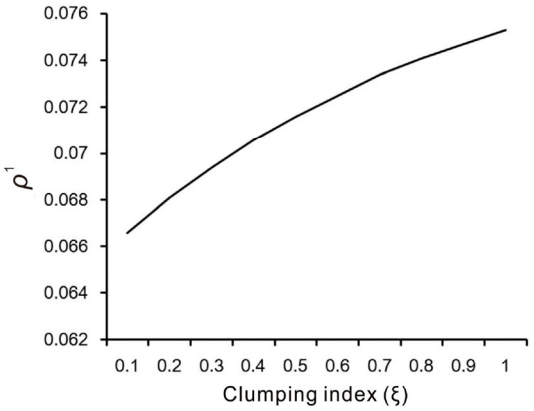

Figure 21 The relationships between clumping indices and ρ^1.

remote sensing models. Using other active remote sensing methods, for example Lidar (light detection and ranging), to cooperate with passive methods will be the trend in the future.

In this study, the clumping index is a key variable to unify different kinds of vegetation. A functional relationship between the clumping index and canopy structural parameters is the basis of the inversion of the vegetation parameters, especially *LAI*. Limited by length of the article, an analytical expression of the clumping index will be discussed in another paper.

Acknowledgements *The authors gratefully appreciate the reviewers for their valuable and insightful comments and suggestions and International Science Editing to polish our paper. This work was supported by the National Natural Science Foundation of China (Grant Nos. 41271346, 41571329 & 41230747) and the Major State Basic Research Development Program of China (Grant No. 2013CB733402).*

References

Chandrasekhar S. 1960. Radiative Transfer. New York: Dover Publications Inc. 53

Chen J M, Leblanc S G. 1997. A four-scale bidirectional reflectance model based on canopy architecture. IEEE Trans Geosci Remote Sens, 35: 1316–1337

Fan W L, Chen J M, Ju W, Zhu G. 2014. GOST: A geometric-optical model for sloping terrains. IEEE Trans Geosci Remote Sens, 52: 5469–5482

Huang D, Knyazikhin Y, Dickinson R E, Rautiainen M, Stenberg P, Disney M, Lewis P, Cescatti A, Tian Y, Verhoef W, Martonchik J V, Myneni R B. 2007. Canopy spectral invariants for remote sensing and model applications. Remote Sens Environ, 106: 106–122

Huang H G, Qin W H, Liu Q H. 2013. RAPID: A radiosity applicable to porous individual objects for directional reflectance over complex vegetated scenes. Remote Sens Environ, 132: 221–237

Jupp D L B, Strahler A H. 1991. A hotspot model for leaf canopies. Remote Sens Environ, 38: 193–210

Knyazikhin Y, Martonchik J V, Myneni R B, Diner D J, Running S W. 1998. Synergistic algorithm for estimating vegetation canopy leaf area index and fraction of absorbed photosynthetically active radiation from MODIS and MISR data. J Geophys Res, 103: 32257–32275

Knyazikhin Y, Schull M A, Xu L, Myneni R B, Samanta A. 2011. Canopy spectral invariants. Part 1: A new concept in remote sensing of vegetation. J Quant Spectrosc Ra, 112: 727–735

Kuusk A. 1991. The hot spot effect in plant canopy reflectance. In: Myneni R B, Ross J, eds. Photon-Vegetation Interactions: Application in Optical Remote Sensing and Plant Physiology. New York: Springer-Verlag. 139–159

Li X, Strahler A H. 1985. Geometric-Optical modeling of a conifer forest canopy. IEEE Trans Geosci Remote Sens, GE-23: 705–721

Liang S. 2005. Quantitative Remote Sensing of Land Surfaces. New York: John Wiley and Sons. 76–134

Mõttus M. 2007. Photon recollision probability in discrete crown canopies. Remote Sens Environ, 110: 176–185

Müller-Linow M, Pinto-Espinosa F, Scharr H, Rascher U. 2015. The leaf angle distribution of natural plant populations: assessing the canopy with a novel software tool. Plant Methods, 11, doi: 10.1186/s13007-015-0052-z

Nilson T. 1971. A theoretical analysis of the frequency of gaps in plant stands. Agric Meteorol, 8: 25–38

North P R J. 1996. Three-dimensional forest light interaction model using a Monte Carlo method. IEEE Trans Geosci Remote Sens, 34: 946–956

Panferov O, Knyazikhin Y, Myneni R B, Szarzynski J, Engwald S, Schnitzler K G, Gravenhorst G. 2001. The role of canopy structure in the spectral variation of transmission and absorption of solar radiation in vegetation canopies. IEEE Trans Geosci Remote Sens, 39: 241–253

Qin W, Gerstl S A W. 2000. 3-D scene modeling of semidesert vegetation cover and its radiation regime. Remote Sens Environ, 74: 145–162

Qin W, Jupp D L B. 1993. An analytical and computationally efficient reflectance model for leaf canopies. Agric For Meteorol, 66: 31–64

Smolander S, Stenberg P. 2005. Simple parameterizations of the radiation budget of uniform broadleaved and coniferous canopies. Remote Sens Environ, 94: 355–363

Stenberg P. 2007. Simple analytical formula for calculating average photon recollision probability in vegetation canopies. Remote Sens Environ, 109: 221–224

Verhoef W. 1984. Light scattering by leaf layers with application to canopy reflectance modeling: the SAIL model. Remote Sens Environ, 16: 125–141

Xu X. 2005. Remote Sensing Physics (in Chinese). Beijing: Peking University Press. 45–121

Yan B Y, Xu X R, Fan W J. 2012. A unified canopy bidirectional reflectance (BRDF) model for row crops. Sci China Earth Sci, 55: 824–836

Zhang R H, Tian J, Li Z L, Su H B, Chen S H, Tang X Z. 2010. Principles and methods for the validation of quantitative remote sensing products. Sci China Ser Earth Sci, 53: 741–751

Zhou X, Tao S, Yao K. 1991. Advanced Atmospheric Physics (in Chinese). Beijing: China Meteorological Press

Zhu X H, Feng X M, Zhao Y S. 2012. Multi-scale MSDT inversion based on LAI spatial knowledge. Sci China Earth Sci, 55: 1297–1305